Colloidal Complexes Obtained from Charged Block Copolymers and Surfactants: A Comparison between Small-Angle Neutron Scattering, Cryo-TEM, and Simulations†

Jean-François Berret* and Pascal Hervé

Complex Fluids Laboratory, Unité Mixte de Recherche CNRS - Rhodia n° 166, 259 Prospect Plains Road CN 7500, Cranbury, New Jersey 08512

Olivier Aguerre-Chariol

Rhodia, Centre de Recherches d'Aubervilliers, 52 rue de la Haie Coq, F-93308 Aubervilliers, Cedex, France

Julian Oberdisse

Laboratoire Léon-Brillouin, CEA Saclay, F-91191 Gif-sur-Yvette, France

Received: December 16, 2002; In Final Form: April 10, 2003

We report on small-angle neutron scattering and cryo-transmission electron microscopy of complexes made from polyelectrolyte-neutral block copolymers and surfactants. Two block copolymer/surfactant systems have been investigated. In the first system, the polyelectrolyte block is negatively charged (poly(sodium acrylate), molecular weight 5 000 g/mol) and the neutral block is a poly(acrylamide) chain of molecular weight 30 000 g/mol. This copolymer is studied in solution in the presence of a cationic surfactant, dodecyltrimethylammonium bromide (DTAB). In the second system, the polyelectrolyte block is positively charged (poly(trimethylammonium ethylacrylate), molecular weight 11 000 g/mol) and the neutral block is again a poly(acrylamide) of molecular weight 30 000 g/mol. This copolymer is studied in solution with an anionic surfactant, sodium dodecyl sulfate (SDS). We show that the diblocks copolymers associate with oppositely charged surfactants into colloidal complexes which have a core−shell microstructure. For the two systems investigated, we have found that the core is constituted from densely packed surfactant micelles, presumably connected by the polyelectrolyte chains. Within the complexes, the DTAB or SDS micelles have the same aggregation number as in aqueous solutions above the cmc. The outer part of the complex is a corona formed by the neutral poly(acrylamide) chains. The microstructure of the core has been inferred from a strong forward neutron scattering and the appearance of a structure peak at high wave vectors ($q_0 \sim 0.16$ Å^{-1}). Using a model of aggregation of colloids developed for latex−silica nanocomposites and based on a Monte Carlo algorithm, we have simulated the internal structure of the aggregates. The model assumes spherical cages containing from one to several hundreds of micelles in a closely packed state. The agreement between the model and the data is remarkable. This allows us to conclude that the structure peak at $q_0 \sim 0.16$ Å^{-1} is associated with the hard-sphere interactions between micelles in the core.

I. Introduction

During the last years, the interactions between nanoparticles and polymers in aqueous solutions have been the subject of numerous theoretical and experimental investigations. A general result is that the phase behavior of the mixed polymer−particle system is strongly modified by the interactions between the species. Stabilization of colloidal suspensions can be achieved, for instance by adsorption of a polymer brush on the surface of the particles. The destabilization of suspensions can be also induced by polymers, and the mechanisms are depletion or polymer bridging.[1] This general scheme applies well to mixed systems composed from polyelectrolytes and oppositely charged surfactant in aqueous solutions. In this case, the surfactant micelles are playing the role of the particles mentioned previously. In the water rich region of the three-components phase diagram, polyelectrolytes and oppositely charged surfactant solutions exhibit a first-order phase transition.[1,2] The phase separation is generally between two or several phases, which can appear as a liquid, as a paste, or as a solid.[3−5] In that later case, the solid phase has the aspect of a precipitate. The occurrence of a liquid−liquid or liquid−solid phase separation is normally determined by the physicochemical properties of the polyelectrolyte/surfactant pair.[3−17] On the other hand, the microscopic mechanism responsible for this transition is not fully understood. Several authors have suggested that the phase separation is associative, with the polyelectrolyte chains playing the role of attractive bridges between micelles.[3−5,18]

When the former homopolyelectrolyte chain is now part of a diblock copolymer, the other block being a neutral and water soluble chain, the phase separation described above ceases to occur.[19−23] Instead, there is the formation of finite size colloids made from both surfactant and copolymers. Based on light and small-angle neutron scattering investigations, we have recently proposed a novel picture for these colloids.[23,24] These colloids have been found to exhibit a core−shell microstructure. The

† Part of the special issue "International Symposium on Polyelectrolytes".

* To whom correspondence should be addressed. E-mail: jeanfrancois.berret@us.rhodia.com.

10.1021/jp027740+ CCC: $25.00
Published on Web 06/10/2003

core is constituted from densely packed surfactant micelles connected between them by polyelectrolyte blocks. The outer part of the colloid is a corona, and it is made from the neutral blocks. In the system consisting of poly(sodium acrylate)-*b*-poly(acrylamide) block copolymer and dodecyltrimethylammonium bromide, we have shown that the core and the corona dimensions could be determined quantitatively from neutron scattering results. We have found for the core and corona radii values around 100 and 500 Å, respectively. The average numbers of micelles and diblocks per particle are comparable and of the order of hundred.

In the present paper, we extend our former investigations and use a copolymer where the first block is a positively charged strong polyelectrolyte and where the surfactant is anionic. By means of small-angle neutron scattering, we demonstrate that this system forms complexes with the same microstructure than the one evidenced previously.[23,24] We also complete the characterization of the complexes using the cryo-transmission electron microscopy technique. The average size of the complexes can be directly deduced from cryo-TEM images, and it is found to compare quite precisely with the neutron scattering determinations. Finally, we have developed a numerical simulation using the Monte Carlo technique in order to calculate quantitatively the scattered intensity arising from an aggregate which models this type of colloid. This aggregate is described as a densely packed assembly of small spheres, the spheres representing the micelles. Using an excluded volume interaction potential between spheres, we have found a good agreement between the experimental and simulated scattering intensities.

II. Experimental Section

Materials and Sample Preparation. In the present work, two block copolymer/surfactant systems have been investigated. In the first system, the polyelectrolyte block is poly(sodium acrylate), a negatively charged and weak polyelectrolyte. The neutral block is a poly(acrylamide) chain. Molecular weights of both blocks are 5000 and 30 000 g/mol, respectively. At neutral pH, which is the pH at which the experiments were conducted, the ionization of the polyelectrolyte blocks is around 75%. This copolymer is studied in solution in the presence of a cationic surfactant, dodecyltrimethylammonium bromide (DTAB). In the second system, the polyelectrolyte block is poly(trimethylammonium ethylacrylate methyl sulfate), a positively charged and strong polyelectrolyte. This polymer is sometimes referred to as poly{[2-(acryloyloxy)ethyl]trimethylammonium methyl sulfate} in the literature.[17,25] For this second system, the neutral block is again a poly(acrylamide). Molecular weight are 11 000 and 30 000 g/mol for the two blocks, respectively. This copolymer is studied in solution with an anionic surfactant, sodium dodecyl sulfate (SDS). Poly(sodium acrylate)−*b*-poly(acrylamide) and poly(trimethylammoniumethylacrylate methyl sulfate)−*b*-poly(acrylamide) block copolymers, hereafter denoted as PANa−PAM and PTEA−PAM, respectively, were synthesized by controlled radical polymerization in solution. The synthesis is based on the Madix technology which consists of a novel transfer agent mediated reaction developed by Rhodia.[26] The chemical specifications of these two polymers (names, abbreviations, molecular weight, average number of monomers and polydispersity index) are summarized in Table 1. The chemical formulas of the monomers are shown in Figure 1. DTAB and SDS were purchased from Sigma and used without further purification. The critical micellar concentrations are 0.46 wt % (15 mmol/l) for DTAB and 0.23 wt % (8 mmol/l) for SDS.

TABLE 1: Chemical Specifications of the Block Copolymers Used in the Present Work[a]

	system 1		system 2	
	PE block	neutral block	PE block	neutral block
abbreviation	PANa	PAM	PTEA	PAM
M_W (g/mol)	5000	30 000	11 000	30 000
nb of monomers	70	420	41	420
PI	1.6		n.d.	
surfactant	DTAB		SDS	

[a] Here, PANa stands for poly(sodium acrylate), PTEA for poly(trimethylammoniumethylacrylate methyl sulfate) and PAM for poly(acrylamide).

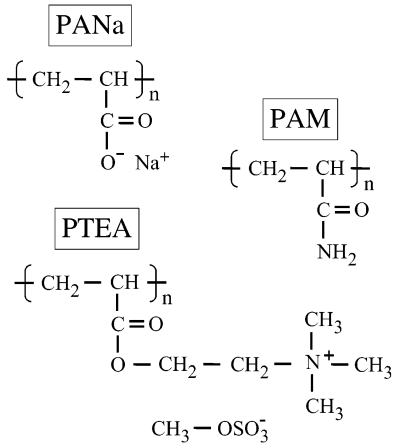

Figure 1. Chemical structure of the polymer blocks investigated in this work. We have used the following terminology: PANa for poly(sodium acrylate), PAM for poly(acrylamide) and PTEA for poly(trimethylammonium ethylacrylate methyl sulfate). This later polymer is sometimes referred to as poly{[2-(acryloyloxy)ethyl]trimethylammonium methyl sulfate} in the literature.[17,25]

The mixed surfactant and polymer solutions are defined by the two parameters, c and Z. c is the total concentration ($c = c_P + c_S$ where c_P and c_S are the weight concentrations in polymer and in surfactant) and Z is the stoechiometric ratio for chargeable groups: $Z = [S]/(n[P])$, where [S] and [P] are the molar concentrations for surfactant and polymer, and n is the average number of monomers in the polyelectrolyte block. $n = 70$ for poly(sodium acrylate) and 41 for poly(trimethylammonium ethylacrylate), see Table 1. $Z = 1$ describes an isoelectric solution, characterized by the same number densities of positive and negative chargeable ions. Mixed copolymer/surfactant solutions at concentration c typically below 30 wt % and at charge ratio Z were prepared by mixing pure surfactant (at c and $Z = \infty$) and pure polymer (at c and $Z = 0$) solutions in the desired amount. Z is proportional to the mass ratio of the two liquids. For the PANa−PAM/DTAB and PTEA−PAM/SDS systems, we observe no phase separation comparable the one of homopolyelectrolyte and oppositely charged surfactant. The solutions appear homogeneous and transparent in the c and Z ranges explored.

Small-Angle Neutron Scattering. Small-angle neutron scattering (SANS) was performed on the D11 and D22 beam lines of the Institute Laue-Langevin (Grenoble, France). PANa−PAM/DTAB and PTEA−PAM/SDS solutions were prepared at a total concentration $c = 0.5\%$ and 1%, varying the charge ratios Z between 0 (pure polymer) and ∞ (pure surfactant). To enhance the scattering contrast, D_2O was used as solvent. The list of the coherent scattering lengths, molecular volumes, and coherent scattering length densities of the chemical species studied in this work are given in Table 2. As shown in the table,

TABLE 2: Coherent Scattering Lengths (b in 10^{-12} cm), Molecular Volumes (V in Å^3), and Coherent Scattering Length Densities (ρ in 10^{10} cm^{-2}) of the Chemical Species Studied in This Work

species	b (10^{-12}cm)	V (Å^3)	ρ (10^{10} cm^{-2})
DTAB	−1.14	486	−0.23
SDS	+1.59	412	+0.39
$CH_2-CHCOOH$	+1.66	114	+1.46
$CH_2-CHCOO^-,Na^+$	+2.40	149	+1.61
$CH_2-CHCOO(CH_2)_2$ $N^+(CH_3)_3;CH_3SO_4^-$	+3.57	358	+1.00
$CH_2-CHCONH_2$	+1.64	105	+1.56
D_2O	+1.915	30	+6.38

all of the chemical species (polymer and surfactant) have a good contrast with respect to D_2O, and thus they are expected to contribute to the total scattering cross section. On D22, the data collected at 2 and 14 m cover a range in wave-vector: 1.5×10^{-3} and 0.25 Å^{-1}, with an incident wavelength of 12 Å. On D11, three settings were used (1.1, 4.5, and 20 m) with a neutron wavelength of 8 Å. The spectra are treated according to the standard Institute Laue-Langevin procedures. Some solutions were studied on the two spectrometers D11 and D22 in order to test the reproducibility and the accuracy of the respective instruments. The absolute scattering cross-sections were found to be in excellent agreement.

Cryo-Transmission Electron Microscopy. Cryo-transmission electron microscopy experiments were performed on the same PANa−PAM/DTAB solutions than those used for neutron scattering (that is the ones made with D_2O). The advantage is then that we are able to compare cryo-TEM images of the colloidal complexes with their signatures in Fourier space. Solutions at concentration $c = 0.5\%$ and charge ratios $Z = 0.5$ and 1 were investigated by this technique. The experimental procedure is described in details in ref 27.

III. Experimental Results

Small-Angle Neutron Scattering. Figure 2 shows the scattering intensity obtained for PANa−PAM/DTAB solutions in D_2O at $c = 1\%$, for $Z = 0$ (pure polymer, lower left graph), 0.2, 0.5, 1, 10, and ∞ (pure surfactant, lower right graph). Increasing the charge ratio modifies profoundly the wave-vector dependencies of the intensity. From $Z = 0.2$ to 0.5, the intensity measured at low wave-vectors passes from ∼0.2 to 1000 cm^{-1}, indicating a huge increase in the size of the scattering particles. For the mixed PANa−PAM/DTAB solutions, there exists a critical stoichiometric ratio (here $Z_C \sim 0.3$[23,24]) above which the scattering intensity is dominated by two noticeable features, a strong forward scattering ($q \rightarrow 0$) and a structure peak at high wave-vectors. This peak is located at $q_0 = 0.165 \pm 0.005$ Å^{-1} and indicated by arrows (Figs. 2). Note that for $Z = 1$ there is a damped oscillation in the intensity decay around 0.05 Å^{-1}. In our first reports, we have shown that these two features are correlated, and that they are the signatures of the form factor of the core−shell aggregates. The strong forward scattering is associated with the overall size of the colloidal complex, and the structure peak at $q_0 = 0.165$ Å^{-1} arises from the strong interactions between micelles in the core. To determine the core sizes, the neutron intensities of the PANa−PAM/DTAB solutions at $c = 1\%$ and Z above 0.5 have been fitted assuming a distribution of spherical and homogeneous particles of average radius R_C and of standard deviation $\sigma(R_C)$.[24] The values for R_C for PANa−PAM/DTAB at $Z = 0.5$, 1, and 10 are shown in Table 3 and these radii are comprised between 110 and 150 Å. In this range of charge ratios, the standard deviation $\sigma(R_C)$ remains constant, around 25 Å. In line with the arguments developed in refs 23 and 24, the external polymer brush scatters much less than the core. Moreover, its contribution becomes apparent only at wave-vectors $q < 0.01$ Å^{-1}.

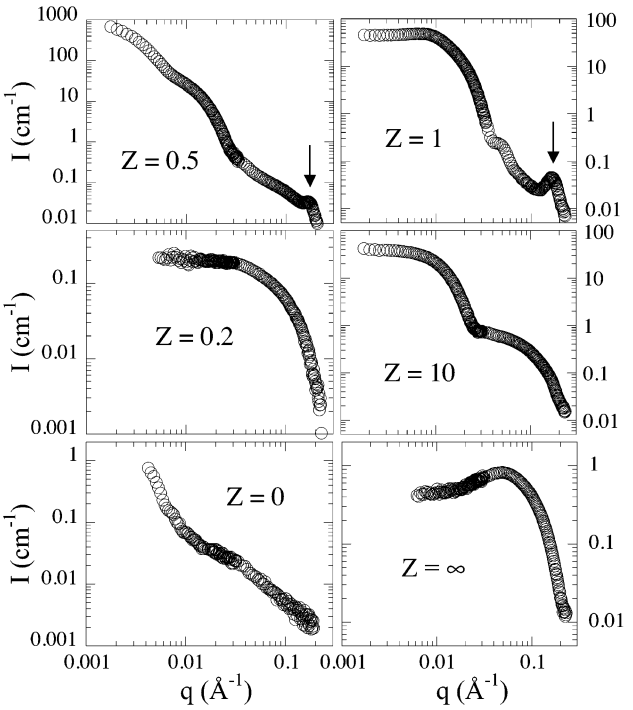

Figure 2. Neutron scattering intensities obtained for PANa−PAM/DTAB aqueous solutions at $c = 1\%$ and $Z = 0$, 0.2, 0.5, 1, 10, and ∞. Pure polymer ($Z = 0$) and pure surfactant ($Z = \infty$) are shown in the lower left and in the lower right graphs, respectively. Note the different scales for each plot and the strong increase in intensity between $Z = 0.2$ and 0.5. At $Z = 1$, an intermicellar structure peak is observed at a wave vector $q_0 = 0.165$ Å^{-1} (indicated by an arrow).

TABLE 3: Core Radius R_C and Standard Deviation $\sigma(R_C)$ of the Colloidal Complexes Made from Neutral/Polyelectrolyte Block Copolymers and Opositely Charged Surfactant[a]

	charge ratio Z	core radius R_C (Å)	standard deviation $\sigma(R_C)$ (Å)
PANa−PAM/DTAB	0.5	136 ± 4	30
$c = 1\%$	1	110 ± 2	17
(data from Figure 2)	10	154 ± 4	27
PTEA-PAM/SDS	1	91 ± 3	15
$c = 1\%$	10	102 ± 3	16
(data from Figure 3)			

[a] The values are determined from neutron scattering at concentration $c = 1$ % (see Figures 2 and 3).

Figure 3 displayed the scattering intensities obtained for PTEA−PAM/SDS solutions in D_2O at $c = 1\%$ at the same Z values (0, 0.2, 0.5, 1, 10, and ∞). To emphasize the similarities between the two systems, the layout of the plot is analogous to that of Figure 2. Pure polymer ($Z = 0$) and pure surfactant ($Z = \infty$) are shown in the lower left and in the lower right graphs, respectively. The analogy between the two systems in terms of the neutron scattering cross-sections is striking, particularly at charge ratios $Z = 1-10$. The strong forward scattering and the structure peak are here recovered. For PTEA−PAM/SDS solutions, the positions of the structure peak is at $q_0 = 0.154 \pm 0.004$ Å^{-1}, corresponding to an intermicellar distance of 40.8 Å. To find out the core sizes of the mixed colloids, we have performed again an analysis of the neutron data in terms

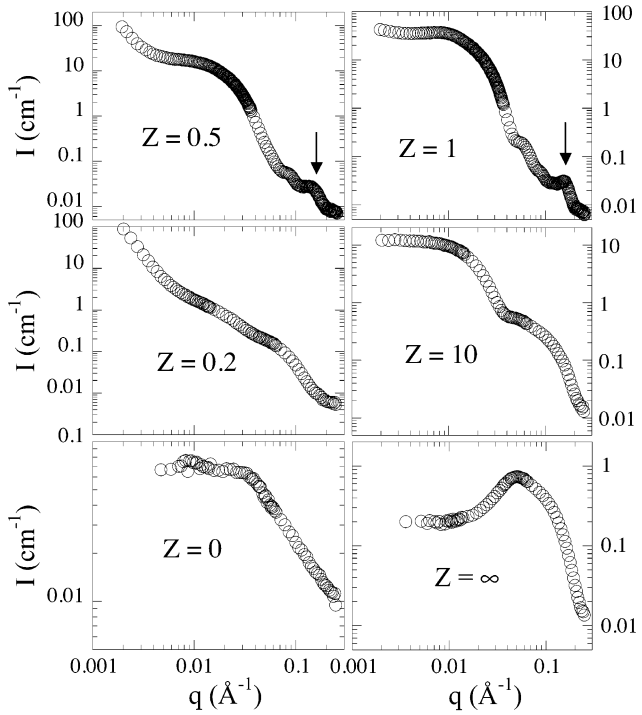

Figure 3. Neutron scattering intensities obtained for PTEA-PAM/SDS aqueous solutions at $c = 1\%$ and $Z = 0$, 0.2, 0.5, 1, 10, and ∞. Pure polymer ($Z = 0$) and pure surfactant ($Z = \infty$) are shown in the lower left and in the lower right graphs, respectively. To emphasize the similarities with the PANa−PAM/DTAB solutions, we used the same layout as in Figure 2. At $Z = 1$, an intermicellar structure peak is observed at a wave vector $q_0 = 0.154 \pm 0.004$ Å^{-1} (indicated by an arrow). It corresponds to an intermicellar distance of 40.8 Å

of distribution of particles of mean radius R_C and standard deviation $\sigma(R_C)$. The R_C values for PTEA−PAM/SDS solutions at $c = 1\%$ and $Z = 1$ and 10 are shown in Table 3. These radii are smaller than the ones estimated for PANa−PAM/DTAB and around 100 Å. From these studies, we conclude that the colloidal complexes obtained from either anionic/neutral or from cationic/neutral block copolymers with oppositely charged surfactant have the same core−shell microstructure.

Cryo-TEM Experiments and Comparison with the SANS Data. Cryo-transmission electron microscopy was performed on two PANa−PAM/DTAB solutions at charge ratios $Z = 0.5$ and 1 ($c = 0.5\%$). These solutions were prepared in D_2O and were investigated by SANS prior to the cryo-TEM experiments. In Figure 4a, we show a cryo-TEM image obtained at $Z = 0.5$. Two types of spherical particles can be distinguished. The majority of these particles have an average diameter of 300 Å, but some are in the range 800−1000 Å (see insets). Figure 4b displays the neutron scattering intensity of the same solution, using a Guinier representation for spherical symmetry ($I(q)$ versus q^2 in semilogarithmic scale). Note that, when plotted in a double logarithmic scale, the data shown in Figure 4b are very much like those of the upper left diagram of Figure 2 ($c = 1\%$). In the Guinier representation, the intensity exhibits two successive exponential decays, indicated by the two straight lines in Figure 4b. The slopes associated to the straight lines correspond to radii of gyration $R_G = 340 \pm 20$ and 117 ± 5 Å. Once transformed in terms of diameters (and assuming that the particles are homogeneous), one ends up with overall sizes of 870 ± 50 and 300 ± 15 Å, respectively. These values are in good agreement with the cryo-TEM results.

At $Z = 1$, cryo-TEM images reveal a unique type of spherical aggregates and their average diameter is around 250 Å (see

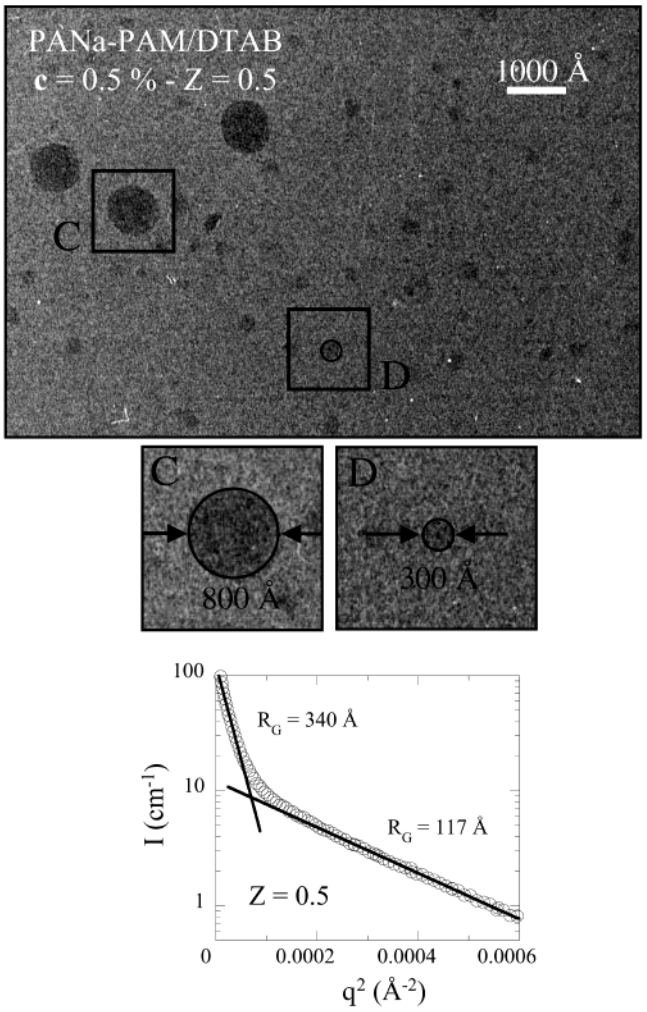

Figure 4. (a) Photograph obtained by cryo-transmission electron microscopy on a PANa−PAM/DTAB solution at the concentration $c = 0.5\%$ and charge ratio $Z = 0.5$. This solution was prepared in D_2O. Aggregates of diameters 300 and 800 Å (see insets) are visible. (b) Guinier representation of the neutron scattering intensity for the same solution. $I(q)$ is shown versus q^2 in a semilogarithmic scale. The two successive exponential decays (indicated by straight lines) correspond to average diameters of 870 ± 50 and 300 ± 15 Å, respectively.

Figure 5a). This result is again confirmed by the neutron scattering data obtained on the same solution. In Figure 5b is plotted the experimental intensity obtained at $c = 0.5\%$, together with the scattering function associated to slightly polydisperse spherical particles of radius $R_C = 106$ Å and a standard deviation $\sigma = 18$ Å. In the intermediate q range, the agreement between the experimental and calculated intensities is satisfactory. The contribution of the corona to the total scattering appears at low wave-vectors by a further increase of the intensity (indicated by an arrow). A schematical representation of the colloids, based on the SANS and cryo-TEM results is shown in Figure 6. More data on the form factor of the aggregates, and especially on the respective weights of the core and corona contributions to the scattering, will be shown in a forthcoming report. We can conclude here that the structural studies of the colloidal complexes in both direct and reciprocal spaces give consistent results. The sizes that are revealed by both techniques are ascribed to the cores of the complexes. The resolution of the cryo-TEM is however not sufficient to observe either the internal structure of the core or the external corona of polyacrylamide chains.

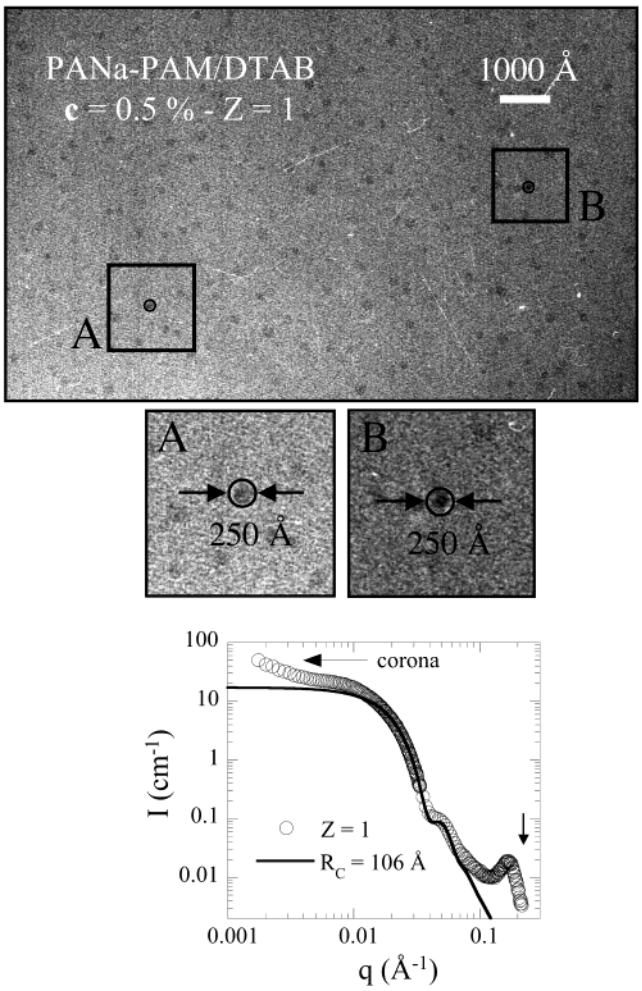

Figure 5. (a) Photograph obtained by cryo-transmission electron microscopy on a PANa−PAM/DTAB solution at the concentration $c = 0.5\%$ and charge ratio $Z = 1$. This solution was prepared in D_2O. Aggregates of diameters 250 Å (insets) are visible. (b) Neutron scattering intensity for the same solution. The continuous line corresponds to the scattering from slightly polydisperse spherical particles of radius $R_C = 106$ Å and a standard deviation $\sigma = 18$ Å.

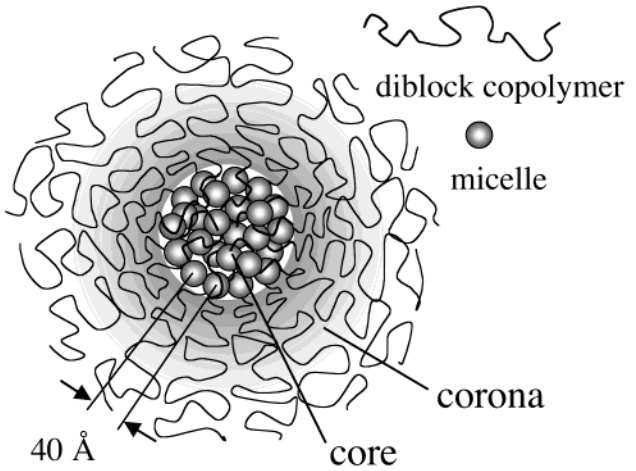

Figure 6. Schematical representation of a colloid complex formed by association of polyelectrolyte/neutral diblocks and oppositely charged surfactants, as deduced from light and neutron scattering measurements.[23,24]

IV. Numerical Simulations

General. Our method consists of constructing a "cage" containing N_{agg} spheres of radius R. These spheres represent the surfactant micelles and the cage models the core of the colloidal complex described previously. In the wave-vector range of interest, the contribution of the polymers to the overall scattering is negligible when compared to that of the micelles, and therefore, it is not taken into account in the simulations. The aggregation number N_{agg} is of the order of one hundred.[23] The cage is chosen to be spherical and of radius $R_C \gg R$. The spheres undergo Brownian motions within the cage, which is simulated by a standard Metropolis algorithm.[28] The structure factor is calculated at regular intervals as time proceeds, and memorized for averaging. This method was originally developed for films of latex-silica nanocomposites.[29]

Micellar Interactions. The volume fraction of spheres ϕ in the cage is given by

$$\phi = N_{agg}\left(\frac{R}{R_C}\right)^3 \tag{1}$$

Because this volume fraction ϕ can be relatively large, we have to consider the interactions between micelles in the cage. The detailed shape of this potential is a priori not known. In the present work, we show simulation results using an excluded volume interaction potential, accounting for hard sphere repulsions[30]

$$V(r) = \infty \qquad \text{for } r < 2R$$
$$V(r) = 0 \qquad \text{elsewhere} \tag{2}$$

where r is the distance between the center-of-mass of neighboring spheres. Other kinds of interaction potentials such as attractive and/or repulsive have been attempted for comparison, and they will be discussed in a separate report.[31]

Initial Configuration. The neutron scattering experiments suggest that the volume fraction of micelles into the core is as high as 50%. Such a large value causes some difficulties in setting up the initial configuration: the cage is then so crowded that it is virtually impossible to place all spheres at random without overlap. There are two options to solve this dilemma. The first one is to place the spheres in an ordered manner. This has the major inconvenience that it might force the system into some structure, which we do not want. We chose the second solution which consists of starting with a larger initial cage, i.e., with a lower initial volume fraction. In practice, the initial volume fraction is set at 20%, the aggregation number N_{agg} and the radius of the spheres R remaining unchanged. There, all spheres can be placed at random without overlap. The system is then concentrated progressively, as the simulation proceeds. During the concentration steps, the particles undergo Brownian motion, as explained in the next paragraph. At regular time intervals, the size of the cage is decreased such that it still contains all of the spheres from the initial configuration. The concentration procedure is stopped once the desired volume fraction of $\phi = 50\%$ is reached.

Monte Carlo Algorithm. The implementation of the Monte Carlo algorithm goes as follows.[28] A sphere is chosen at random and moved in a random direction by a distance d. The total energy of the system, expressed in units of k_BT, is calculated before and after the step. If the energy difference ΔE is negative, i.e., if the energy has decreased, the step is accepted. For positive ΔE, the step is also accepted if $\exp(-\Delta E)$ is greater than a random number drawn from a uniform distribution between 0 and 1. The running average of the fraction of rejected steps is continuously monitored, and the step distance d is adjusted (within bounds) in order to reach a preset value for this ratio. Steps that break the nonoverlap condition for the spheres as

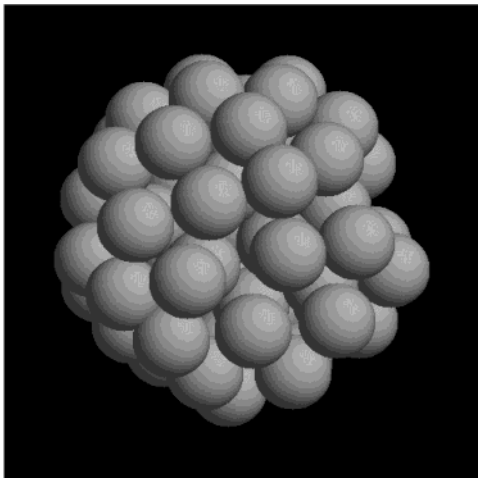

Figure 7. Typical snapshot of an aggregate at the end of a Monte Carlo simulation. The overall aggregate (radius R_C) is characterized by a volume fraction of small spheres of 50% and an aggregation number $N_{agg} = 60$. Within the aggregate, the spheres undergo Brownian motions and interact via an excluded volume potential (eq 2).

well as those leading a micelle out of the cage are rejected. Figure 7 presents a typical snapshot of an aggregate at the end of the concentration procedure. It is characterized by a volume fraction of 50% and an aggregation number $N_{agg} = 60$.

Calculation of the Scattered Intensity. The neutron scattering cross-section of a solution containing a number density n of spheres per unit volume can be expressed as

$$I(q) = nV^2\Delta\rho^2 S(q,N_{agg})F(q,R) \qquad (3)$$

where $F(q,R)$ is the form factor of a sphere and $S(q,N_{agg})$ is the structure factor arising from the spheres belonging to a same cage. $\Delta\rho$ is the contrast with respect to that of the surrounding solvent and $V = 4/3\pi R^3$ is the volume of a sphere. In this approach, we neglect the interactions between cages. Because by definition the form factor $F(q,R)$ in eq 3 goes to unity as q goes to 0, we deduce for the structure factor the equality $S(q \rightarrow 0,N_{agg}) = N_{agg}$. The structure factor $S(q,N_{agg})$ in eq 3 is calculated from the Fourier transform of the pair distribution function obtained from the simulation. It involves the positions r_i of all N_{agg} spheres in the cage at the moment of calculation. Once the concentration procedure described in the preceding paragraphs is completed, such as $\phi = 50\%$, $S(q,N_{agg})$ is calculated every $10\times N_{agg}$ Monte Carlo steps according to

$$S(q,N_{agg}) = 1 + \frac{1}{N_{agg}}\sum_{i\neq k}^{N_{agg}} \frac{\sin[q(r_i - r_k)]}{q(r_i - r_k)} \qquad (4)$$

The final structure factor is obtained by averaging over the intermediate structure factors derived during this last phase of the simulation. To summarize, we can say that for the calculation of the structure factor associated to a cage, instead of averaging over many cages of various shapes, we average on the time during which the Brownian spheres explore a large number of configurations within a single cage. In the ergodic approximation, these two approaches (averaging on space or time) are equivalent.

The neutron scattering experiments suggest that the colloidal complexes are slightly polydisperse. We have introduced a distribution function $P(N_{agg},N_{agg}^{av},\Delta N_{agg})$ for the aggregation numbers, where N_{agg}^{av} and ΔN_{agg} are the average aggregation number and standard deviation of the distribution. The average

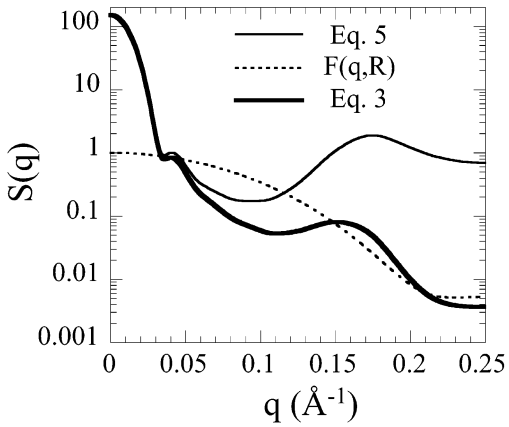

Figure 8. Thin continuous curve: structure factor $S(q,N_{agg}^{av},\Delta N_{agg})$ of an aggregate calculated from the Fourier transform of the pair distribution function obtained from the simulation. Calculations were made using eqs 4 and 5, $R = 20.7$ Å, $N_{agg}^{av} = 126$, and $\Delta N_{agg} = 55$. Dashed curve: form factor of the spheres smeared out by the polydispersity. Continuous thick curve: product of the two previous functions. As a result, a maximum is observed at large wave-vectors that is around 0.16 Å^{-1}.

interparticle structure factor then replaces the expression of $S(q,N_{agg})$ in eq 3

$$S(q,N_{agg}^{av},\Delta N_{agg}) = \frac{1}{N_{agg}^{av}}\int N_{agg}P(N_{agg},N_{agg}^{av},\Delta N_{agg}) \times S(q,N_{agg})\, dN_{agg} \qquad (5)$$

Note then that the value of the structure factor at zero scattering angle is no more equal to the average aggregation number N_{agg}^{av}, but to $\langle N_{agg}^2\rangle/N_{agg}^{av}$. Inspired again by experiments, we have described the polydispersity of the elementary spheres through a Gaussian centered on $\langle R\rangle = 20.7\text{Å}$ and of standard deviation $\langle R^2 - \langle R\rangle^2\rangle^{1/2} = 2.6$ Å.

Results of a typical simulation are shown in Figure 8. The average structure factor $S(q,N_{agg}^{av},\Delta N_{agg})$ is calculated according to eq 4 and 5 using $R = 20.7$ Å, $N_{agg}^{av} = 126$, and $\Delta N_{agg} = 55$. It is shown as a continuous thin line. The distribution function $P(N_{agg},N_{agg}^{av},\Delta N_{agg})$ has been chosen such as to correspond to a Gaussian distribution for the cage radii, as suggested by the neutron data ($R_C = 128$ Å and $\sigma(R_C) = 18$ Å).[23,24] The dashed curve in Figure 8 represents the form factor of the elementary spheres. The first oscillation of the form factor expected at 0.22 Å^{-1} is here considerably smeared out by the polydispersity. The continuous thick curve in Figure 8 finally displays the product of the averaged structure and form factors. As a result, a maximum is observed at large wave vectors, around 0.16 Å^{-1}. In Figure 9, the results of the previous simulation are compared to data obtained on a PANa−PAM/DTAB solution at $c = 1\%$ and $Z = 2$ in a semilogarithmic scale. The inset shows the same data in double logarithmic scales. The calculated intensity of Figure 8 has been shifted by an arbitrary factor in order to fit the experimental data. The overall agreement between the two sets of data is excellent, especially concerning the damped oscillation around 0.05 Å^{-1} and the position and width of the structure peak at large wave vectors. The weak structure factor peak centered around 0.007 Å^{-1} (Figure 9) and arising from the complex−complex interactions is of course not reproduced, as we have a priori excluded all such interactions in the simulations.

V. Conclusions

In this paper, new results on the complexation of polyelectrolyte/neutral block copolymers and oppositely charged sur-

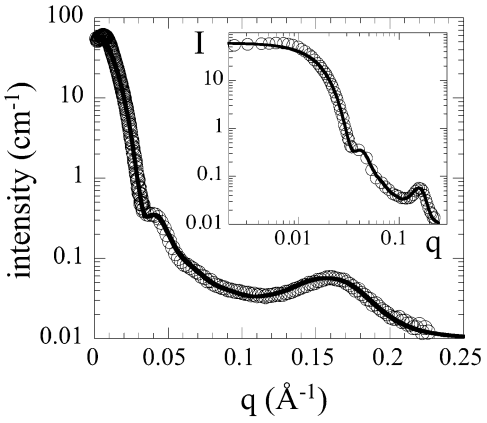

Figure 9. Comparison between the simulation results and the neutron scattering intensity obtained on a PANa−PAM/DTAB solution at $c =$ 1% and $Z = 2$ in a semilogarithmic scale. The inset shows the same data in double logarithmic scales. The calculated intensity in Figure 8 (thick continuous curve) has been shifted by an arbitrary factor in order to fit the experimental data. The parameters of the simulation are the same as in Figure 8.

factants are shown and analyzed. We have extended our former experiments performed on poly(sodium acrylate)−*b*-poly(acrylamide)/dodecyltrimethylammonium to a system made of a cationic/neutral block copolymer with an anionic surfactant. This new system is a 11 000−30 000 poly(trimethylammonium ethylacrylate methyl sulfate)−*b*-polyacrylamide, and the surfactant is sodium dodecyl sulfate. SANS shows that for charge ratios $Z > 1$ the microstructure of the colloidal complexes in both systems are identical and consistent with a core−shell organization. The core is constituted from densely packed surfactant micelles, presumably connected by the polyelectrolyte blocks. Within the complexes, the DTAB or SDS micelles have the same aggregation number (∼70) as in aqueous solutions. The outer part of the complex is a corona formed by the neutral poly(acrylamide) chains. The microstructure of the core has been inferred from a strong forward neutron scattering ($q \rightarrow 0$) and the appearance of a structure peak at high wave vectors (0.16 Å^{-1}). This structure peak is associated with the mean distance between surfactant micelles in the core. For Z comprised between the critical charge ratio Z_C and 1, we have noticed that the colloidal complexes exhibit a bimodal distribution with maxima centered around 300 and 1000 Å (Figure 4a). This result was confirmed by dynamic light scattering experiments.[24] It seems that, at these intermediate values of Z, the corona which appears during the complex formation is not sufficient to stabilize the aggregates and limit their growth. We have no explanation for the bimodal size distribution in this regime. New experiments varying the molecular weigths of both polyelectrolyte and neutral blocks are under progress and should give new insight into this phenomenon. Cryo-transmission electron microscopy was used in addition to neutron scattering. Some experiments were performed on the same solutions using the two techniques. Cryo-TEM data confirm accurately the SANS results, as well as the bidisperse distribution mentioned previously.

Finally, we have developed a numerical simulation using the Monte Carlo technique which allows us to calculate the scattered intensity arising from a particle which is a densely packed assembly of spheres. These spheres represent the surfactant micelles. These attempts were made in order to check the interpretation of the neutron spectra on a more quantitative basis. In the wave-vector range of interest, $q = 10^{-2}$ to 4×10^{-1} Å^{-1}, the contribution of the block polymers was not taken into account. With Monte Carlo simulations, we are able to adjust the calculated scattering to the experimental neutron data with a reasonable set of parameters. The agreement between the experimental and simulated scattering form factors of the colloidal complexes is remarkable. We are for instance able to confirm that the structure peak observed at large wave-vectors, as anticipated, arises from the hard-sphere interactions between the micelles located in the core. During the course of this work, we have been aware of two recent reports, one by Li and co-workers[32] and one by Gérardin and co-workers[33] on similar systems. These authors have studied the complexation of polyelectrolyte/neutral block copolymers with oppositely charged multivalent counterions[32] and with lanthanum-based nanoparticles.[33] In both systems, it is found that the block copolymers self-assemble into micelle-like aggregates presenting a core−shell microstructure. Their results show strong similarities with those quoted in the present paper.

Acknowledgment. We thank L. Picullel, D. Roux, B. Cabane, M. Joanicot, and M. Morvan for fruitful discussions and comments. We are also grateful to Ronny Eng for his assistance and support during the experiments. Financial support from the Laboratoire Léon Brillouin (Saclay, France) and from the Institute Laue-Langevin (Grenoble, France) is also acknowledged.

References and Notes

(1) Spalla, O. *Curr. Opin. Colloid Interface Sci.* **2002**, *7*, 179.
(2) *Polymer-Surfactant Systems*; Kwak, J. C. T., Ed.; Marcel Dekker: New York, 1998; Vol. 77.
(3) Ilekti, P.; Piculell, L.; Tournilhac, F.; Cabane, B. *J. Phys. Chem. B* **1998**, *102*, 344.
(4) Ilekti, P.; Martin, T.; Cabanne, B.; Piculell, L. *J. Phys. Chem. B* **1999**, *103*, 9831.
(5) Svensson, A.; Piculell, L.; Cabanne, B.; Ilekti, P. *J. Phys. Chem. B* **2002**, *106*, 1013.
(6) Thalberg, K.; Lindman, B.; Bergfeldt, K. *Langmuir* **1991**, *7*, 2893.
(7) Antonietti, M.; Conrad, J. *Angew. Chem., Int. Ed. Engl.* **1994**, *33*, 1869.
(8) Hansson, P.; Almgren, M. *Langmuir* **1994**, *10*, 2115.
(9) Kahandurina, Y. V.; Dembo, A. T.; Bogacheva, V. B.; Zezin, A. B.; Kabanov, V. A. *Polym. Sci.* **1994**, *36*, 189.
(10) Bronstein, L. M.; Platonova, O. A.; Yakunin, A. N.; Yanovskaya, I. M.; Dembo, A. T.; Makhaeva, E. E.; Mironov, A. V.; Khokhlov, A. R. *Langmuir* **1998**, *14*, 252.
(11) Sokolov, E.; Yeh, F.; Khokhlov, A.; Grinberg, V. Y.; Chu, B. *J. Phys. Chem. B* **1998**, *102*, 7091.
(12) Zhou, S.; Yeh, F.; Burger, C.; Chu, B. *J. Phys. Chem. B* **1999**, *103*, 2107.
(13) Ashbaugh, H. S.; Lindman, B. M. *Macromolecules* **2001**, *34*, 1522.
(14) Dembo, A. T.; Starodoubtsev, S. G. *Macromolecules* **2001**, *34*, 2635.
(15) Kogej, K.; Evmenenko, G.; Theunissen, E.; Berghmans, H.; Reynaers, H. *Langmuir* **2001**, *17*, 3175.
(16) Zhou, S.; Hu, H.; Burger, C.; Chu, B. *Macromolecules* **2001**, *34*, 1772.
(17) Bergström, M.; Kjellin, U. R. M.; Cleasson, P. M.; Pedersen, J. S.; Nielsen, M. M. *J. Phys. Chem. B* **2002**, *106*, 11412.
(18) Hansson, P. *Langmuir* **2001**, *17*, 4167.
(19) Bronich, T. K.; Kabanov, A. V.; Kabanov, V. A.; Yui, K.; Eisenberg, A. *Macromolecules* **1997**, *30*, 3519.
(20) Bronich, T. K.; Cherry, T.; Vinogradov, S.; Eisenberg, A.; Kabanov, V. A.; Kabanov, A. V. *Langmuir* **1998**, *14*, 6101.
(21) Kabanov, A. V.; Bronich, T. K.; Kabanov, V. A.; Yu, K.; Eisenberg, A. *J. Am. Chem. Soc.* **1998**, *120*, 9941.
(22) Bronich, T. K.; Popov, A. M.; Eisenberg, A.; Kabanov, V. A.; Kabanov, A. V. *Langmuir* **2000**, *16*, 481.
(23) Hervé, P.; Destarac, M.; Berret, J.-F.; Lal, J.; Oberdisse, J.; Grillo, I. *Europhys. Lett.* **2002**, *58*, 912.
(24) Berret, J.-F.; Cristobal, G.; Hervé, P.; Oberdisse, J.; Grillo, I. *Eur. J. Phys. E* **2002**, *9*, 301.
(25) Cleasson, P. M.; Bergström, M.; Dedinaite, A.; Kjellin, M.; Legrand, J.-F.; Grillo, I. *J. Phys. Chem. B* **2000**, *104*, 11689.
(26) Taton, D.; Wilczewska, A.-Z.; Destarac, M. *Macromol. Rapid Commun.* **2001**, *22*, 1497.
(27) In, M.; Aguerre-Chariol, O.; Zana, R. *J. Phys. Chem. B* **1999**, *103*, 7747.

(28) Metropolis, N.; Rosenbluth, A. W.; Rosentbluth, M. N.; Teller, A. M.; Teller, E. *J. Chem. Phys.* **1953**, *21*, 1087.

(29) Oberdisse, J.; Demé, B. *Macromolecules* **2002**, *35*, 4397.

(30) Klein, R.; D′aguanno, B. Static Scattering Properties of Colloidal Suspensions. In *Light Scattering, Principles and Developments*; Brown, W., Ed.; Oxford: New York, 1996; p 30.

(31) Oberdisse, J. *Europhys. Lett.* **2003**, in preparation.

(32) Li, Y.; Gong, Y.-K.; Nakashima, K.; Murata, Y. *Langmuir* **2002**, *18*, 6727.

(33) Bouyer, F.; Gérardin, C.; Fajula, F.; Puteaux, J.-L.; Chopin, T. *Colloids Surf. A* **2003**, in press.